IOP Publishing Journal of Optics
J. Opt. **20** (2018) 015401 (12pp) https://doi.org/10.1088/2040-8986/aa9b05

Study of the retardance of a birefringent waveplate at tilt incidence by Mueller matrix ellipsometer

Honggang Gu, Xiuguo Chen, Chuanwei Zhang, Hao Jiang[1] and Shiyuan Liu[1]

State Key Laboratory of Digital Manufacturing Equipment and Technology, Huazhong University of Science and Technology, Wuhan 430074, People's Republic of China

E-mail: hjiang@hust.edu.cn and shyliu@hust.edu.cn

Received 31 July 2017, revised 23 October 2017
Accepted for publication 16 November 2017
Published 12 December 2017

Abstract

Birefringent waveplates are indispensable optical elements for polarization state modification in various optical systems. The retardance of a birefringent waveplate will change significantly when the incident angle of the light varies. Therefore, it is of great importance to study such field-of-view errors on the polarization properties, especially the retardance of a birefringent waveplate, for the performance improvement of the system. In this paper, we propose a generalized retardance formula at arbitrary incidence and azimuth for a general plane-parallel composite waveplate consisting of multiple aligned single waveplates. An efficient method and corresponding experimental set-up have been developed to characterize the retardance versus the field-of-view angle based on a constructed spectroscopic Mueller matrix ellipsometer. Both simulations and experiments on an MgF_2 biplate over an incident angle of 0°–8° and an azimuthal angle of 0°–360° are presented as an example, and the dominant experimental errors are discussed and corrected. The experimental results strongly agree with the simulations with a maximum difference of 0.15° over the entire field of view, which indicates the validity and great potential of the presented method for birefringent waveplate characterization at tilt incidence.

Keywords: birefringent waveplate, retardance, field-of-view error, ellipsometry and polarimetry, instrumentation, measurement, metrology

(Some figures may appear in colour only in the online journal)

Nomenclature

θ	the incident angle of polarized light, i.e. the angle between the incident ray and the normal of the waveplate;
α	the azimuthal angle of polarized light, i.e. the angle between the incident plane and the x-axis of the coordinate system;
φ	field-of-view angle of incident light, i.e. the angle between the incident ray and the x-axis of the coordinate system;
φ_e	field-of-view angle of refracted light for the extraordinary ray (e-ray), i.e. the angle between the e-ray and the x-axis of the coordinate system;
θ_e	the refraction angle for the e-ray;
k	the index of the single waveplate in the order of wave propagation;
θ_{xk}, θ_{yk}	the refraction angles for the x-component and the y-component of polarized light in the k^{th} single waveplate, respectively;
L	the optical path difference (OPD) between the o-rays and e-rays in the waveplate;

[1] Authors to whom any correspondence should be addressed.

L_k	the OPD between the o-ray and the e-ray in the k^{th} single waveplate;
d	the thickness of the waveplate;
d_k	the thickness of the k^{th} single waveplate;
n_{e}, n_{o}	the major refractive indices for the e-ray and the o-ray, respectively;
n_{ek}, n_{ok}	the major refractive indices for the e-ray and the o-ray in the k^{th} single waveplate, respectively;
n_{xk}, n_{yk}	the refractive indices for the x-component and the y-component of polarized light in the k^{th} single waveplate, respectively;
n	the refractive index for the e-ray at oblique incidence $n(\theta, \alpha)$;
Δn	the birefringence of the birefringent crystal $\Delta n = n_{\text{e}} - n_{\text{o}}$;
δ	the retardance of the birefringent waveplate.

1. Introduction

Waveplates made of birefringent materials are widely used for the polarization modulation of polarized light by introducing a phase shift (also known as retardance or retardation) between the two orthogonal polarization components (i.e. the ordinary and extraordinary rays (o-ray and e-ray respectively)). They are indispensable elements in various optical systems, such as polarimetry/ellipsometry [1–3], interferometry [4, 5], etc. and the performance of these systems heavily depends on the waveplate polarization properties [6–10]. Among these properties, retardance is an intrinsic and important optical characteristic of a birefringent waveplate. For a birefringent material, such as quartz and magnesium fluoride (MgF_2), the effective refractive index for the e-ray, as well as the optical path difference (OPD) between the o-ray and the e-ray, depends on the angle between the wave normal of the incident light and the optical axis [11, 12]. Thus, the retardance of a birefringent waveplate will change with the angle of the incident light with respect to the optical axis of the plate, named the field-of-view angle in this paper. Usually, a waveplate is designed and applied with a nominal retardance for a normal incident condition. However, in practical applications, the waveplate is always at oblique incidence due to imperfect manufacturing, installation and adjustment, and non-collimation of the conical optical path in imaging systems [3, 13]. Under these non-ideal incident conditions, the retardance of the birefringent waveplate will deviate from its nominal value, which indubitably has great influence on the final performance of the system. Therefore, it is of great importance to study the field-of-view errors on the retardance of a birefringent waveplate, and its characterization method for an arbitrary field-of-view angle.

Many researchers have studied the trajectory and optical path of the e-ray in birefringent materials at oblique incidence. In most of these works, formulas based on the ray tracing method are used to calculate the optical path. For example, Simon derived a formula for the finite ray tracing of uniaxial crystals when the optical axis was normal to the refracting surface directly from Maxwell's equations [14–16]. Hale and Day proposed an approximate expression to study the variation of the retardance of a birefringent waveplate with the direction of propagation, and pointed out that the variation arises from both the optical path length and the refractive index of the e-ray [12]. Chipman studied the mechanics of polarization ray tracing, and compared the difference among different polarization representations, including the polarization ray tracing calculus, the Jones calculus, and the Mueller calculus [17]. Based on the phase matching conditions, Liang [18] and Zhang [19] presented ray tracing formulas for uniaxial crystals and biaxial crystals, respectively. Zhang further derived a formula to calculate the phase shift of birefringent waveplates, including a single waveplate and a compound waveplate [20]. Some researchers studied the transformation properties for a tilted birefringent waveplate when its optical axis was parallel to the plate surface using the Jones matrix method [21, 22]. Avendano-Alejo *et al* applied Huygens's principle to derive equations for tracing the e-ray in a uniaxial crystal when the optical axis was normal to the retracting surface, as well as when the optical axis was arbitrarily oriented [23–25]. They further used the developed theory to calculate the optical path difference between the ordinary and extraordinary wavefronts for a uniaxial plate [26]. Veiras *et al* presented a general and explicit formula to calculate the phase shift in uniaxial media for any angle of incidence, plane of incidence, and direction of the optical axis, by using Maxwell's equations and boundary conditions without any approximation [27]. Most recently, Aleman-Castaneda and Rosete-Aguilar considered the small deviation from orthogonality, and derived a closed-form expression for the angle between polarizations of the o-ray and the e-ray in uniaxial crystals [28]. All these published theories and formulas are valid in order to trace the trajectory and to calculate the optical paths in birefringent materials. Moreover, some researchers further addressed the calculation of the retardance of birefringent waveplates at oblique incidence. However, most of these retardance formulas are specific to simple waveplates at certain incident conditions, such as a single waveplate with its optical axis lying on the incident plane, which cannot be applied to more complicated composite waveplates designed for broadband and hyper-NA imaging systems [2, 13, 29].

Another key issue in the study of the field-of-view errors of a birefringent waveplate is the retardance measurement of the waveplate at an arbitrary incident angle and azimuth angle. Although various techniques have been applied to characterize the polarization properties of a birefringent waveplate, as reviewed by Zhang *et al* [30], only a few of them can be applied to measure the retardance of a waveplate at oblique incidence. Lo *et al* proposed a series of heterodyne interferometers (polariscopes) based on different techniques

to measure the phase retardance as well as the principle axis of a tilted waveplate [31–35]. Chou *et al* developed a phase-sensitive heterodyne polarimeter (ellipsometer) and applied it to characterize the phase retardance of an optically active waveplate and a multi-order waveplate versus the incident angle [36–38]. Williams described a precise measurement of the retardance using rotating-polarizer and rotating-waveplate polarimeters [3, 39]. Most recently, Chakraborty *et al* studied the effect of tilt on the performance of linear retarders by detecting the flux ratio of the orthogonally polarized light from a polarizing beam splitter [40, 41]. These techniques are suitable for the characterization of the retardance for a birefringent waveplate at oblique incidence with relatively high precision. However, most of them directly detect the intensity or the intensity ratio, and need additional techniques (such as phase-locking and light splitting techniques) to complete the measurement, and appropriate algorithms to extract the phase retardance from the detected signals. It is worth pointing out that West and Smith have comprehensively studied the polarization errors associated with birefringent waveplates, including the field-of-view errors, the thickness error, the optic axis tilt errors, and the fast axis misalignment error. They also proposed equipment to measure the absolute retardance of a waveplate by using three Glan–Thompson polarizers, a Soleil-Babinet compensator, a multiline HeNe laser source, and a photomultiplier tube detector. Although various simulations and experiments have been carried out and discussed in their work, little theoretical details are presented. Further, too many elements, including at least the Glan–Thompson polarizers and the Soleil-Babinet compensator, need to be precisely aligned and calibrated, which significantly increases the complexity and the risk of various systematic errors for the retardance measurement system. The Mueller matrix ellipsometer (MME) has been developed as a powerful tool for the characterization of anisotropic samples by providing the full 4×4 Mueller matrix [42, 43], from which the complete polarization parameters, including the retardance, axis orientation, rotary angle, diattenuation as well as the depolarization of the sample, can be achieved [44]. Therefore, the MME will be a promising instrument to characterize the polarization properties of a birefringent waveplate at an arbitrary field-of-view angle.

In this paper, we studied the field-of-view errors on the retardance of a birefringent waveplate using a spectroscopic MME. Firstly, we constructed a generalized formula for the retardance of a general plane-parallel composite waveplate consisting of multiple aligned single waveplates with arbitrary incidence and arbitrary azimuth. The formula is derived by calculating the OPD between the wave normals of the e-rays and o-rays through the composite waveplate based on the ray tracing method and Snell's law. We proposed an MME-based method for the fast and accurate characterization of the retardance of a birefringent waveplate under an arbitrary incident angle and an arbitrary azimuth angle. A corresponding experimental set-up is established based on a home-made MME and high-precision automatic rotators to perform the experiments. Both simulations and experiments on the retardance of a MgF_2 biplate over the incident angle of 0°–8° and azimuth angle of 0°–360° are presented as an example to ascertain whether the experiments agree with the theories. The main sources of the systematic errors in the experiments are discussed and corrected. The maximum deviation between the experiments and the simulations achieved after correction is reduced to 0.15° over the entire field of view, which is one order of magnitude smaller than that before correction. Oscillations in retardance versus incident angle and azimuth angle, as well as spectral performance under different field-of-view angles, are presented and discussed. The results clearly demonstrated some intrinsic characteristics of the field-of-view errors on the retardance of a birefringent waveplate. The fairly strong agreement between the simulations and experiments indicates the validity and great potential of the presented method on the characterization of the birefringent waveplate.

2. Theory

A birefringent crystal has different refractive indices in the directions parallel with and perpendicular to the optical axis, which is one of the most commonly used materials for waveplate (also known as an optical retarder) fabrication. Figure 1 shows the refractive index ellipsoid in the cartesian coordinate system for a uniaxial birefringent crystal, which has only one optical axis, such as quartz, MgF_2, calcite, etc.

In a uniaxial birefringent crystal, the refractive indices in the directions parallel with and perpendicular to the optical axis are named the extraordinary refractive index n_e and the ordinary refractive index n_o, respectively. A plane-parallel waveplate is usually a slice of birefringent crystal polished with the optical axis lying in the plate plane. When propagating in the waveplate, a polarized light is divided into two orthogonal components oscillating along with the optical axis and a direction perpendicular to the optical axis respectively —the former one is an e-ray and the latter one is an o-ray. The two rays have different velocities due to different refractive indices. Thus, a phase shift, also referred to as the retardance or retardation of the waveplate, is introduced between the two orthogonal components, which can be calculated by

$$\delta = \frac{2\pi}{\lambda} L, \tag{1}$$

where λ refers to the vacuum wavelength, and L is the OPD between the two orthogonal components of the polarized light. When the waveplate is under normal incidence of the light, which is the usual condition a waveplate is designed for, the OPD in equation (1) can be specialized as

$$L = \Delta n \cdot d, \tag{2}$$

where $\Delta n = (n_e - n_o)$ is the birefringence of the crystal, and d refers to the effective thickness of the waveplate.

It is known that the field-of-view angle of the light greatly influences the effective refractive indices of the

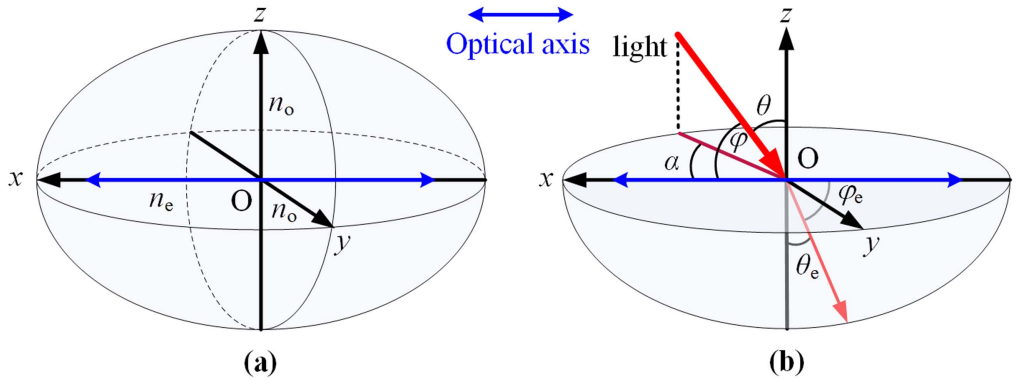

Figure 1. (a) The refractive index ellipsoid of a uniaxial birefringent crystal. The optical axis is parallel with the x-axis, and n_e and n_o are the extraordinary refractive index and the ordinary refractive index, respectively. (b) The propagation of the e-ray in the crystal under arbitrary incidence θ and azimuth α of the light.

birefringent crystal. Specifically, for a uniaxial crystal, the refractive index for the e-ray will vary with the angle of incidence, while the refractive index for the o-ray will remain constant n_o. As depicted in figure 1(b), when the light propagates into the birefringent crystal at an oblique incidence, the effective refractive index for the e-ray can be calculated from [11]

$$\frac{1}{n^2} = \frac{\sin^2\varphi_e}{{n_e}^2} + \frac{\cos^2\varphi_e}{{n_o}^2}, \tag{3}$$

where φ_e is the intersection angle between the optical axis and the wave normal of the e-ray. According to Snell's law and the geometric relationships shown in figure 1(b), we have

$$\sin\theta = n\sin\theta_e, \tag{4}$$

$$\cos\varphi = \sin\theta\cos\alpha = n\sin\theta_e\cos\alpha = n\cos\varphi_e, \tag{5}$$

where θ is the intersection angle between the normal of the x–y plane and the wave normal of the incident light, α refers to the azimuth of the incident plane with respect to the optical axis, θ_e is the refraction angle for the e-ray. Thus, by combining equations (3)–(5), we can obtain

$$\begin{aligned} n &= n_e\left[1 + \left(\frac{1}{{n_e}^2} - \frac{1}{{n_o}^2}\right)\cos^2\varphi\right]^{\frac{1}{2}} \\ &= n_e\left[1 + \left(\frac{1}{{n_e}^2} - \frac{1}{{n_o}^2}\right)\sin^2\theta\cos^2\alpha\right]^{\frac{1}{2}}. \end{aligned} \tag{6}$$

Since the effective refractive indices as well as the propagation lengths change with the incidence and azimuth, the OPD formula given by equation (2) fails when the waveplate is under oblique incidence. Without loss of generality, we study the field-of-view errors on the retardance of a composite waveplate consisting of multiple aligned single waveplates. As is schematically shown in figure 2, the light enters the waveplate at an arbitrary incidence with respect to the normal of the plate plane and an arbitrary azimuth with respect to the x-axis. The plate plane is parallel with the x–y plane, and the optical axes of the single waveplates are parallel with the x-axis or the y-axis. Thus, the incident polarized light is divided into two polarized components oscillating along the x-axis and y-axis respectively, referred to as the x-component and

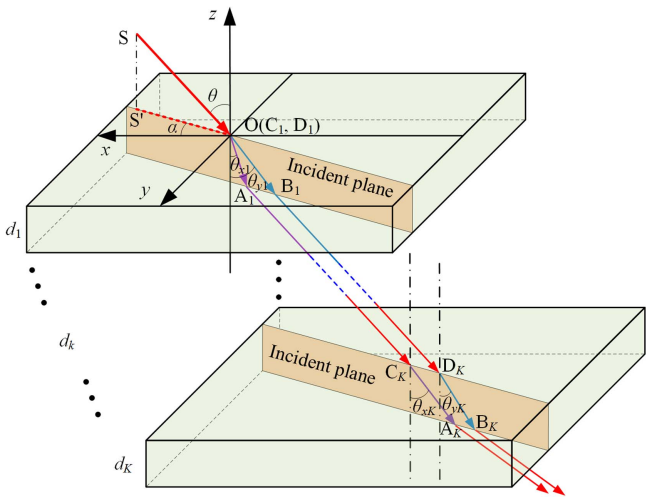

Figure 2. Schematic of the wave normal propagation in a composite waveplate under an arbitrary incidence and an arbitrary azimuth of the incident light.

the y-component for convenience. The single waveplates are numbered 1, 2, …, K in the order of light propagation. **SO** and **S′O** are the wave normal of the incident light and its projection on the plate plane. $\mathbf{C}_k\mathbf{A}_k$ and $\mathbf{D}_k\mathbf{B}_k$ refer to the wave normals for the x-component and the y-component of the polarized light in the k^{th} single-waveplate, and θ_{xk} and θ_{yk} are their refraction angles, respectively.

The retardance of the composite waveplate is given by the sum of the OPDs in the single waveplates

$$\delta = \sum_{k=1}^{K}\frac{2\pi}{\lambda}L_k, \tag{7}$$

According to the geometric relationships in figure 2, the OPD between the x-component and the y-component in the k^{th} single waveplate can be calculated by

$$\begin{aligned} L_k &= n_{xk}|\mathrm{C}_k\mathrm{A}_k| - n_{yk}|\mathrm{D}_k\mathrm{B}_k| + (|\mathrm{C}_k\mathrm{D}_k| - |\mathrm{A}_k\mathrm{B}_k|)\sin\theta \\ &= d_k\left[\frac{n_{xk}}{\cos\theta_{xk}} - \frac{n_{yk}}{\cos\theta_{yk}} + (\tan\theta_{yk} - \tan\theta_{xk})\sin\theta\right], \end{aligned} \tag{8}$$

where θ is the incident angle of the light (i.e. the intersection angle between the normal of the plate plane and the wave normal of the incident light), d_k ($k = 1, 2, \ldots, K$) is the thickness of the k^{th} single waveplate, and n_{xk} and n_{yk} are the effective refractive indices for the x-component and the y-component of the k^{th} single waveplate. Further, according to Snell's law, we have

$$\sin\theta = n_{xk}\sin\theta_{xk} = n_{yk}\sin\theta_{yk}. \tag{9}$$

Thus, equation (8) can be rewritten as

$$L_k = d_k(\sqrt{n_{xk}^2 - \sin^2\theta} - \sqrt{n_{yk}^2 - \sin^2\theta}). \tag{10}$$

From equations (3)–(6), when the optical axis of the k^{th} waveplate is parallel with the x-axis, the effective refractive indices can be given by

$$\begin{cases} n_{xk} = n_{ek}\left[1 + \left(\dfrac{1}{{n_{ek}}^2} - \dfrac{1}{{n_{ok}}^2}\right)\sin^2\theta\cos^2\alpha\right]^{\frac{1}{2}}, \\ n_{yk} = n_{ok} \end{cases} \tag{11a}$$

or when the optical axis of the k^{th} waveplate is parallel with the y-axis

$$\begin{cases} n_{xk} = n_{ok} \\ n_{yk} = n_{ek}\left[1 + \left(\dfrac{1}{{n_{ek}}^2} - \dfrac{1}{{n_{ok}}^2}\right)\sin^2\theta\sin^2\alpha\right]^{\frac{1}{2}}. \end{cases} \tag{11b}$$

In equation (11), n_{ek} and n_{ok} are the extraordinary and the ordinary refractive indices at normal incidence for the k^{th} waveplate, where α refers to the azimuth angle of the incident light, i.e. the angle between the projection of the light on the plate plane and the x-axis.

For a single waveplate, the retardance formula presented in equations (7)–(11) can be specialized in forms consistent with references [26, 27]. In this paper, a compound zero-order waveplate is selected as an example to study the field-of-view errors on the retardance. The compound zero-order waveplate is composed of two multi-order single waveplates made of the same material, whose axes are aligned perpendicular to each other. Here, we assume that the optical axis of the thicker multi-order single waveplate is parallel with the x-axis, and that of the thinner one is parallel with the y-axis. According to the above description and derivation, the retardance of the compound zero-order waveplate under arbitrary incidence and azimuth can be calculated by

$$\begin{aligned} \delta(\theta, \alpha) = {} & \frac{2\pi}{\lambda}d_1\left(\sqrt{{n_e}^2 - \frac{{n_e}^2\cos^2\alpha + {n_o}^2\sin^2\alpha}{{n_o}^2}\sin^2\theta}\right. \\ & \left. - \sqrt{{n_o}^2 - \sin^2\theta}\right) - \frac{2\pi}{\lambda}d_2 \\ & \times\left(\sqrt{{n_e}^2 - \frac{{n_e}^2\sin^2\alpha + {n_o}^2\cos^2\alpha}{{n_o}^2}\sin^2\theta}\right. \\ & \left. - \sqrt{{n_o}^2 - \sin^2\theta}\right), \end{aligned} \tag{12}$$

where d_1 and d_2 are the thicknesses of the thicker single waveplate and the thinner single waveplate, n_e and n_o are the extraordinary refractive index and the ordinary refractive index of the birefringent material, θ and α are the incident angle and the azimuth angle of the light.

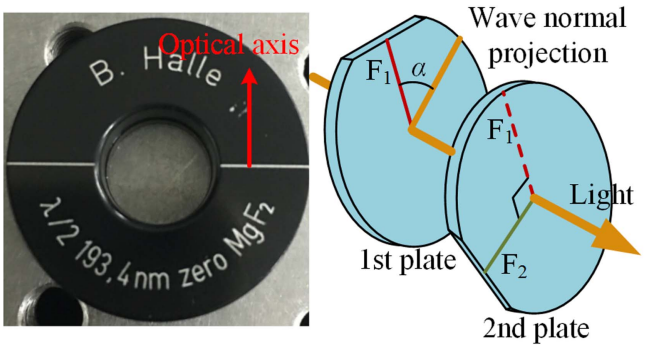

Figure 3. A photograph (left) and schematic (right) of the zero-order MgF_2 biplate tested in this paper.

It should be noted that the formulas presented above do not consider the interference effect introduced by the interface between the waveplates. In practice, it is really difficult to put the single waveplates together without air gap or epoxy resin between them; then the interference effect is inevitable [45]. Although the interference effect may always exist, we ignore its influence on the retardance calculation in this paper due to the following reasons. Firstly, in the fabrication of a compound waveplate, the single waveplates directly contact each other using the optical cement method [2] and are coated with anti-reflective films, which can almost eliminate the interference resulting from the multiple reflections between the interfaces of the waveplate. Secondly, the interference effect on the retardance of the waveplate exhibits a very high-frequency oscillation from the nominal value [45], which is hardly detected by instruments with a general spectral resolution, such as a spectroscopic ellipsometer. Lastly, the interference effect may become extremely complex when the waveplate is under oblique incidence, and a discussion of the weak but complex interference effect is beyond the scope of this paper.

3. Experiment set-up

In this paper, the MgF_2 biplate is tested by a constructed MME to ascertain whether the experimental results agree with the presented formula for the retardance under oblique incidence. The MgF_2 biplate is a commercial zero-order half-wave retarder at 193 nm (RZM 2.10 from B. halle Nachfl. GmbH, Germany). Figure 3 shows a photograph of the product as well as a schematic diagram of the biplate retarder. It consists of two multi-order single waveplates made of MgF_2 which are assembled with their optical axes in a crossed position to construct a linear retarder. The retarder is supplied in a cylindrical mount engraved with the average direction of the optical axis, which is determined by the thicker single waveplate. The extraordinary and the ordinary refractive indices of MgF_2 can be calculated by Sellmeier's equations [46]. The total thickness of the biplate is approximately 1.6 mm. According to equations (1)–(2), we can obtain that

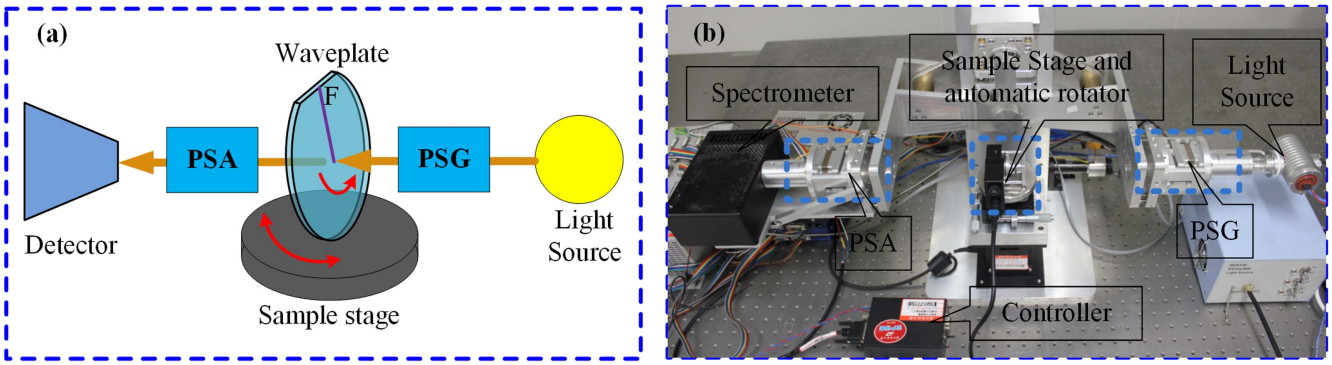

Figure 4. (a) Schematic and (b) platform of the experiment set-up based on the constructed MME.

the effective thickness (i.e. the difference between the thicknesses of the two multi-order single waveplates for a compound zero-order biplate) of the biplate is 7.09 μm, and the designed thicknesses of the two single waveplates are $d_1 = 807.09$ μm and $d_2 = 800.00$ μm. With these conditions, the retardance of the biplate at normal incidence is about 90° at a wavelength of 347 nm.

The retardance of the waveplate is measured by a straight-through MME system, as schematically shown in figure 4(a). The experimental system consists of a light source, a polarization state generator (PSG), a sample stage, a polarization state analyzer (PSA) and a detector [2]. The waveplate to be tested is mounted in a rotation holder and then placed on the sample stage. Both the sample stage and the rotation holder can be automatically rotated within a range of 0°–360° to adjust the incidence angle and the azimuth angle of the light entering the waveplate. The PSG contains a polarizer followed by a rotating compensator, while the PSA contains a second rotating compensator followed by an analyzer. The two compensators of the PSG and PSA continuously rotate synchronously with coupled frequencies of $\omega_1 : \omega_2 = 5 : 3$ to modulate and analyze the polarized light. By performing Fourier analysis of the modulated intensity signal detected by the detector, the complete 4×4 Mueller matrix of the waveplate can be obtained, and then the retardance of the waveplate can be solved from the Mueller matrix [44]. By adjusting the sample stage and the rotation holder, we can obtain the retardances of the waveplate under different incidence angles and azimuth angles.

Figure 4(b) shows the platform of the experimental set-up based on a constructed MME. In the device, the light source is a deuterium and quartz tungsten halogen combined source. The polarizer and the analyzer are α-BBO Rochon prisms. The rotating-compensators are homemade achromatic retarders and the detector is a commercial spectrometer. With these components used in the constructed MME, the available wavelengths cover a range of 200–1000 nm. The constructed MME has been set up with strict system calibration to ensure the performance in the measurement of the Mueller matrix. The measurement accuracy and precision of the Mueller matrix over the whole spectral range are better than 0.2% and 0.1%, respectively. Two measurement modes, i.e. the straight-through measurement mode and the reflective measurement mode, can be chosen by rotating the PSG arm and the PSA arm of the ellipsometer simultaneously. In this paper, the MgF_2 biplate is measured in the straight-through measurement mode.

The biplate to be tested is mounted on a high-precision automatic hollow rotator from OptoSigma controlled by a single-axis controller from OptoSigma with the highest resolution of 0.0025°. As shown in figure 4, the biplate is mounted in a holder for protection and then connected to the turntable of the rotator, and then is placed on the sample stage of the MME. The sample stage is a combination of basic contact slide stages and rotation stages, which guarantee six degrees of freedom, i.e. horizontal and vertical movement, horizontal tilt adjustment and rotation around the vertical axis. With these conditions, the sample stage can be attentively adjusted to ensure the light spot totally propagates through the biplate at normal incidence. The rotation of the sample stage around the vertical axis is achieved by a high-precision automatic rotator, also from OptoSigma, with the highest resolution of 0.0025°. Thus, the incident angle and azimuth angle of the polarized light entering the biplate can be selected by controlling the two rotators. A computer connected to the controllers and the ellipsometer is used to control the stage movements and to process the data.

4. Results and discussion

In the experiment, the sample stage is firstly adjusted attentively to guarantee the initial condition of normal incidence (i.e. the incident angle of the light is zero). This condition can be judged by the extreme point in the retardance over a range of rotation and tilt angles around the normal incidence when the azimuth angle of the biplate is not fixed at 45° or 135°. On the other hand, the azimuth angle can be roughly judged from the engraved line on the protecting frame of the biplate, as shown in figure 3. With these judgments of the initial conditions and the help of high-precision automatic rotators, the incident angle and the azimuth angle of the probing light entering the biplate can be precisely controlled and selected.

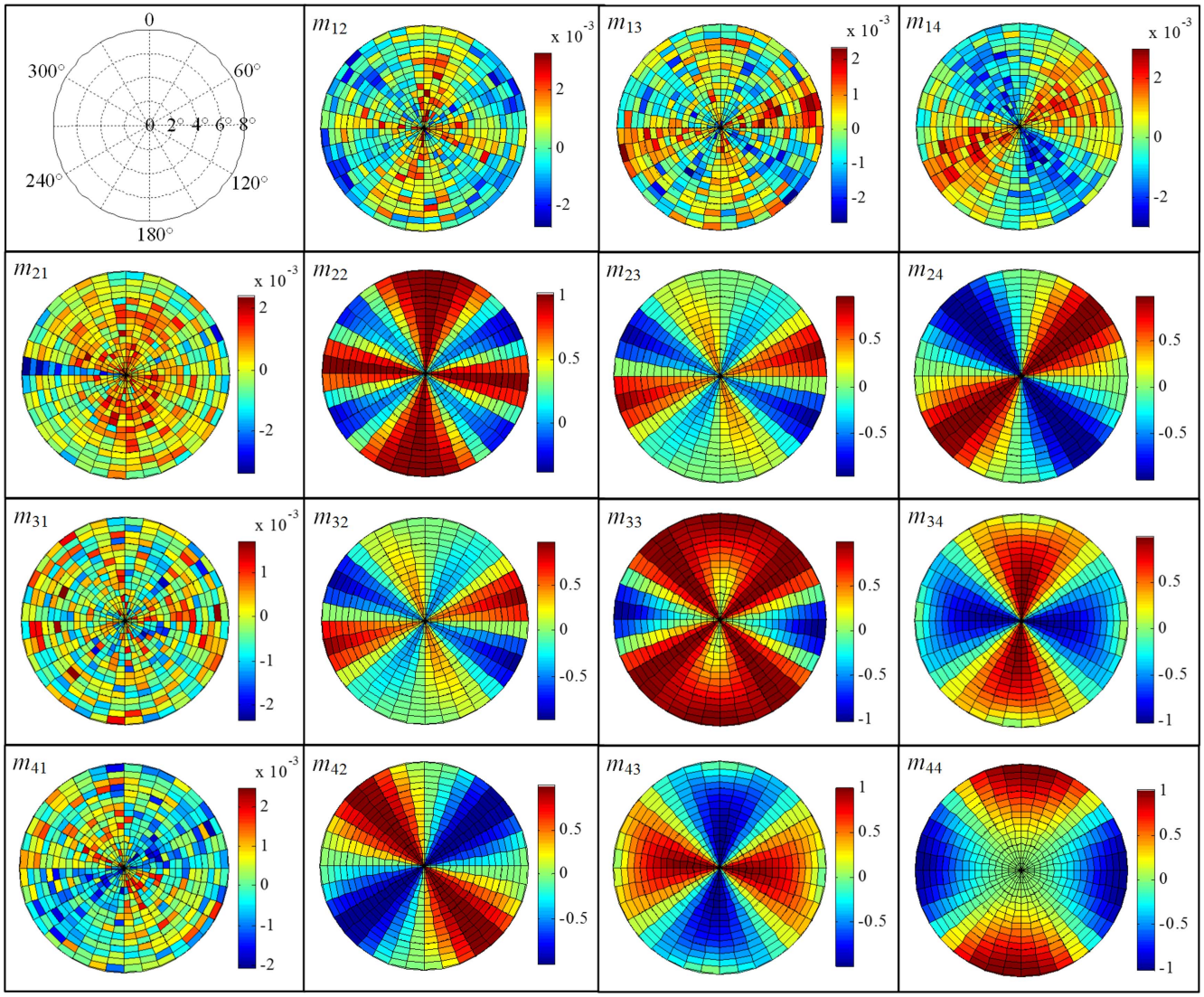

Figure 5. Measured Mueller matrix of the MgF_2 biplate versus field-of-view angle at a wavelength of 347 nm in a polar coordinate system, and the polar radius and polar angle are the incidence and the azimuth, respectively. The Mueller matrix elements have been normalized by the first element m_{11}, and the coordinate system is shown in the upper left corner.

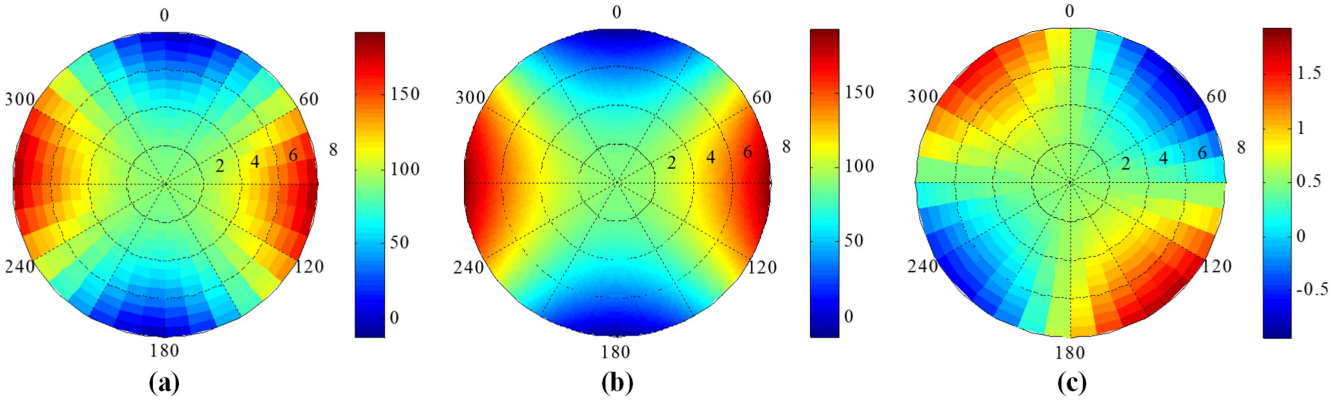

Figure 6. Retardance versus the field-of-view angle at a wavelength of 347 nm in the polar coordinate system (a) experimental results; (b) simulated results; (c) difference between the experiments and the simulations.

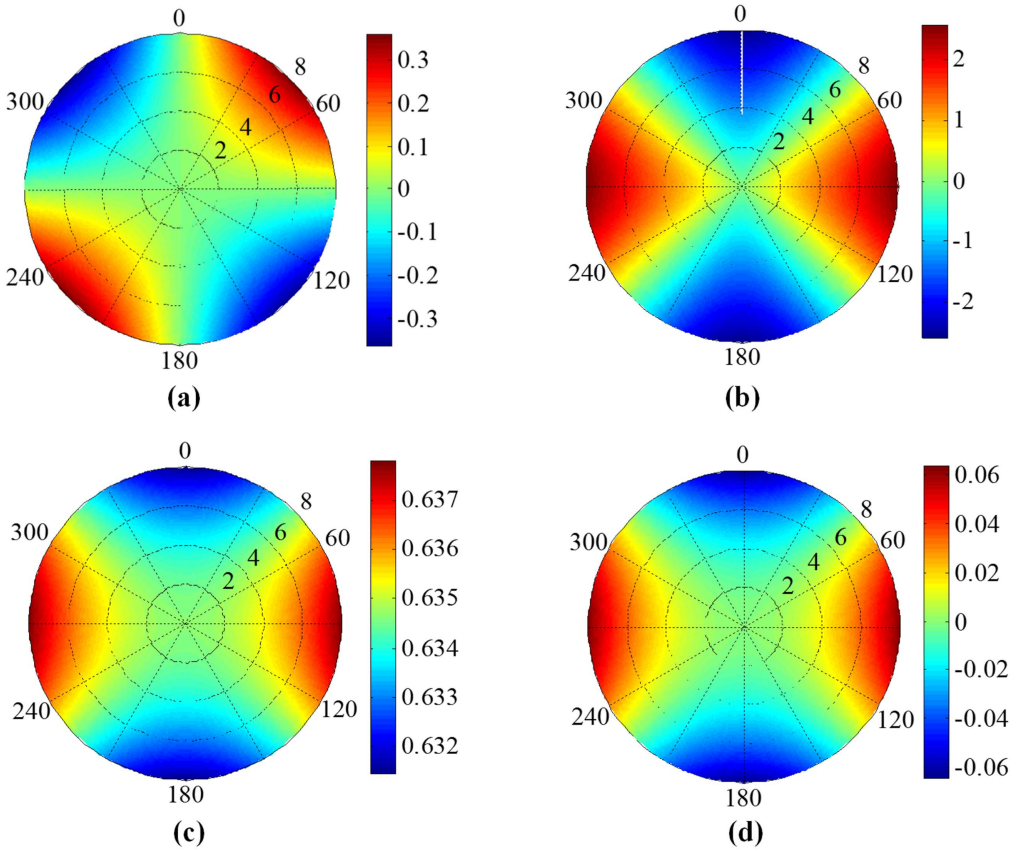

Figure 7. Retardance changes versus different systematic errors in (a) the azimuth angle ($\Delta\alpha = 0.1°$); (b) the incident angle ($\Delta\theta = 0.1°$); (c) the effective thickness ($\Delta(d_1 - d_2) = 0.05\ \mu$m); (c) the total thickness ($\Delta d_1 = \Delta d_2 = 0.5\ \mu$m).

Then the retardances of the MgF_2 biplate under different field-of-view angles can be measured. Here, we present the results over the incident angle of 0°–8° and azimuth angle of 0°–360°, as shown in figures 5–10.

Figure 5 shows the normalized Mueller matrix of the MgF_2 biplate versus the field-of-view angle at a wavelength of 347 nm in the polar coordinate system. It can be seen from figure 5 that the elements in the first row and the first column of the Mueller matrix are approximately zero, and they do not deviate with the field-of-view angle. However, the elements in the bottom right 3×3 matrix block regularly deviate from -1 to 1 with the field-of-view angle. The results in figure 5 indicate that the MgF_2 biplate remains a linear retarder when the incident angle changes, but its retardance varies with the incidence and the azimuth. The Mueller matrix of the MgF_2 biplate can be written as

$$\mathbf{M} = \mathbf{R}(-\alpha)\mathbf{M}(\delta)\mathbf{R}(\alpha) = \begin{bmatrix} 1 & 0 & 0 & 0 \\ 0 & \cos^2(2\alpha) + \sin^2(2\alpha)\cos\delta & \cos(2\alpha)\sin(2\alpha)(1 - \cos\delta) & -\sin(2\alpha)\sin\delta \\ 0 & \cos(2\alpha)\sin(2\alpha)(1 - \cos\delta) & \sin^2(2\alpha) + \cos^2(2\alpha)\cos\delta & \cos(2\alpha)\sin\delta \\ 0 & \sin(2\alpha)\sin\delta & -\cos(2\alpha)\sin\delta & \cos\delta \end{bmatrix}, \tag{13}$$

where α and δ are the azimuth and the retardance of the biplate, respectively. When the waveplate is at oblique incidence, the retardance changes with the incidence as well as the azimuth, but the azimuth will not change with the incidence. The retardance can be obtained from the measured Mueller matrix according to equation (13).

Figure 6 illustrates the experimental retardance, the simulated results, and the difference between the experiment and the simulation over the whole field of view at a wavelength of 347 nm. The simulated results are calculated according to equation (12) using the designed values of thickness. The nominal retardance at a wavelength of 347 nm at normal incidence is about 90°. It can be observed from figure 6 that the deviation in the retardance from its nominal value increases when the incident angle increases, and exhibits a periodicity of 180° versus the azimuth angle. The waveform of the retardance difference between the experiment and the simulation, as demonstrated in figure 6(c), also exhibits a periodicity of 180° versus the azimuth angle. But there is a 45° phase shift between the waveforms of the retardance difference (as shown in figure 6(c)) and those of the retardance (as shown in figures 6(a) and (b)). The

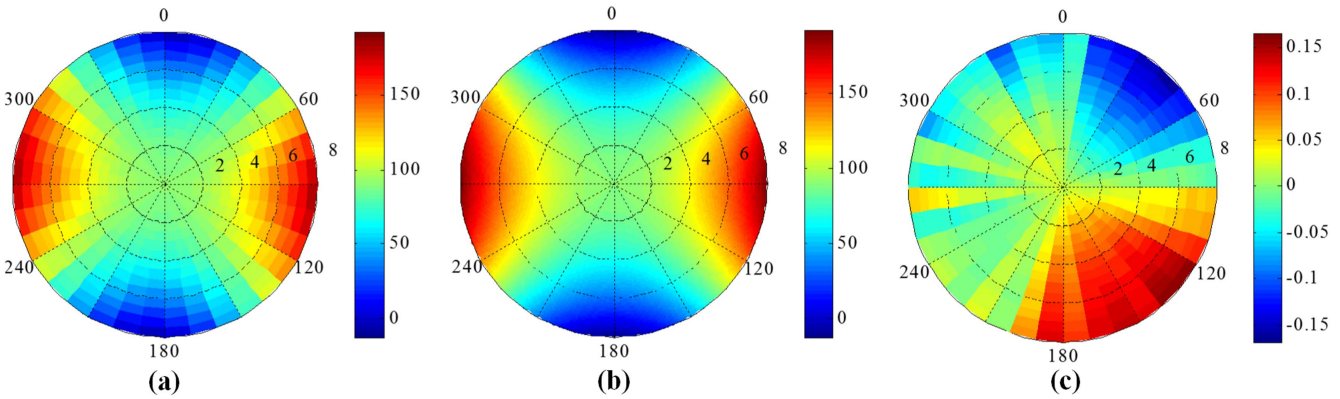

Figure 8. Retardance versus the field-of-view angle at a wavelength of 347 nm after correction (a) experimental results; (b) simulated results after correction; (c) difference between experiments and simulations.

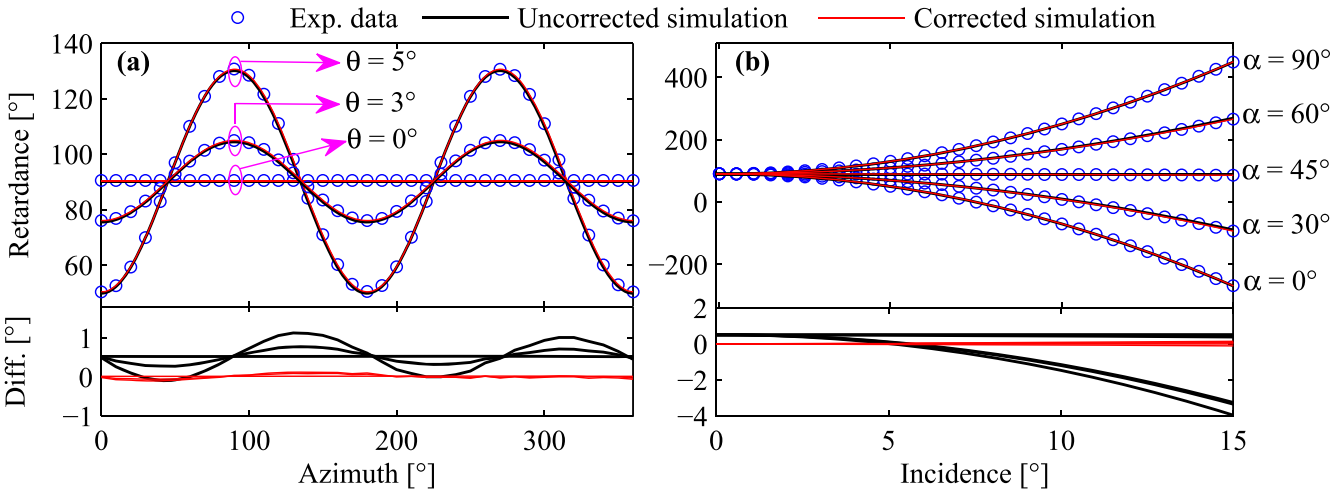

Figure 9. Experimental, uncorrected simulated and corrected simulated results of the oscillations in the retardance of the MgF_2 biplate (top), and the differences between the exeperiments and the simulations (bottom). The wavelength is 347 nm, at which the nominal retardance is about 90°. (a) Retardance oscillations versus the azimuth under different incident angles; (b) retardance oscillations versus the incident angle at different azimuth angles.

maximum value of the retardance difference between the experiment and the simulation is about 2°. Further, there seems to be a DC offset of about 0.5° in the image of the retardance difference. These characteristics in the retardance difference indicate that there may be some significant systematic errors in the experiment.

To ascertain the main source of the errors in the experiment, we simulate the changes in the retardance when small errors exist in the azimuth angle, the incident angle, the effective thickness and the total thickness of the biplate, as shown in figure 7. These simulations are performed according to equation (12) at a wavelength of 347 nm. It can be seen that the errors in the azimuth angle and the incident angle result in periodic changes (with a period of 180°, the same as that shown in figure 6) in the retardance with the azimuth angle, while the error in the effective thickness results in a DC shift in the retardance; the retardance change resulting from a small error in the total thickness of the biplate can be ignored. Further, the oscillation waveform of the retardance change caused by the error in the azimuth angle (as shown in figure 7(a)) exhibits the same phase with the waveform of the retardance difference (as shown in figure 6(c)). However, there is a 45° phase shift between the oscillation waveform of the retardance change caused by the error in the incident angle (as shown in figure 7(b)) and the waveform of the retardance difference (as shown in figure 6(c)). Thus, it can be concluded that the dominant errors resulting in the difference between the experiment and simulation stem from the azimuth angle and the effective thickness of the biplate. Here, we provide an explanation regarding this conclusion from the perspective of experiment settings. In the experiment, the initial condition of normal incidence can be strictly guaranteed by attentive adjustment of the sample stage, and thus the incident angle can be precisely known. However, the initial azimuth is judged by the engraved line on the protecting frame, which is a rough mark of the biplate optical axis, and thus the azimuth angle may contain errors. In addition, the thicknesses of the biplate inevitably introduce errors due to imperfect manufacturing of the single waveplates.

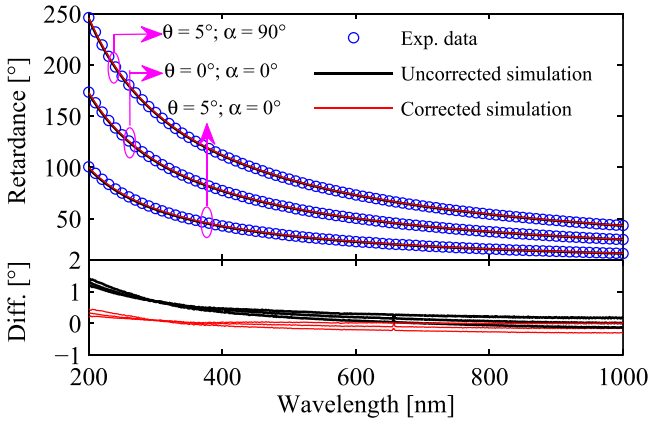

Figure 10. Experimental, uncorrected simulated and corrected simulated results of the vibrations in the retardance of the MgF_2 biplate (top) and the differences between the exeperiments and the simulations (bottom) over the whole wavelength range of 200–1000 nm under different field-of-view angles.

We assume that the initial azimuth is $-0.36°$ and a deviation of 0.04 μm from the designed value exists in the effective thickness of the biplate. Therefore, an offset of $-0.36°$ is added to the azimuth angle, and the effective thickness of the biplate is $d_1 - d_2 = 7.13\ \mu$m in the calculation. After correcting the errors in the azimuth angle and the effective thickness, we recalculate the retardance over the whole field of view, as shown in figure 8. It can be seen from figure 8(c) that the maximum retardance difference between the experiment and the simulation after correction is about 0.15°, which is reduced by more than one order of magnitude compared with that before correction. The residual difference between the experiments and simulations can be attributed to errors in the manufacturing process and the axis alignment of the biplate, the residual errors in the experiment settings, the nonuniformity in the thickness and imperfections in the material of the biplate, and the measurement errors of the MME. For example, the MME may introduce a random error up to 0.05° in the retardance measurement. A discussion of the residual errors is beyond the scope of this paper.

In order to more clearly present and analyze the retardance deviations versus the incident angle and the azimuth angle, the curves shown in figures 6 and 8 are reproduced in the Cartesian coordinate system, as shown in figure 9. It can be seen from figure 9(a) that the retardance exhibits obvious sinusoidal oscillations versus the azimuth angle when the biplate is at oblique incidence. The amplitude of the oscillation increases with the incident angle, while the period remains a constant of 180°. The retardance shows positive deviations from its nominal value within the azimuth range of $45° + i \times 180° \sim 135° + i \times 180°$; shows negative deviations from its nominal value within the azimuth range of $-45° + i \times 180° \sim 45° + i \times 180°$; and remains the nominal value at the azimuth angle of $45° + i \times 180°$ and $135° + i \times 180°$, where i is an integer. As demonstrated in figure 9(b), the deviations in retardance exhibit an accelerated increase with an increase in the incident angle, and the sign of the deviation as well as the value of the acceleration are related to the azimuth angle. From the difference between the experiments and the simulations shown in the bottom of figure 9, it can be observed that a DC offset and systematic vibrations exist in the retardance before correction. Besides, a small error in the azimuth will result in significant deviations in the practical retardance from its theoretical value when the incidence is larger than 5°. An error of 0.36° in the azimuth can cause an error of about 5° in the retardance when the incidence is 15°. Moreover, the retardance is more sensitive to azimuth errors when the azimuth is $45° + i \times 90°$, and less sensitive to azimuth errors when the azimuth is $i \times 90°$, where i is an integer. After compensating the dominant errors in the experiments, the theoretical calculations show extremely strong agreement with the experiments, which verifies the validity of the presented method to characterize the retardance under an arbitrary field-of-view angle.

We also demonstrate the measured and simulated results of the retardance spectra over a wavelength range of 200–1000 nm under different field-of-view angles, as shown in figure 10. Since the refractive indices as well as the birefringence of the material change more violently towards the ultraviolet band, the spectral curves of the retardances as well as the differences between experiments and simulations become steeper when the wavelength becomes shorter. Moreover, when the biplate is at oblique incidence, the deviation in the retardance from its nominal value increases when the wavelength decreases. As shown in the bottom of figure 10, the retardance differences between the experiments and simulations after correction are obviously smaller than those before correction. The differences among the retardance–difference curves of different field-of-view angles over a wavelength range around 350 nm are smaller than those over other wavelength ranges. This can be explained by the fact that the initial conditions of the experimental settings and the corrections of the systematic errors are both performed at a wavelength of 347 nm. This implies that there must be other error sources associated with the wavelength in the experiments, which can be most possibly attributed to the difference between the refractive indices of the practical material and those calculated by Sellmeier's equations.

5. Conclusions

In this work, a general formula is proposed for the retardance calculation of a plane-parallel composite waveplate consisting of multiple aligned single birefringent plates at an arbitrary field-of-view angle. Further, an MME-based method is introduced to characterize the retardance of a birefringent waveplate at oblique incidence. Also, an experimental set-up based on a constructed spectroscopic MME and high-precision automatic rotators is established. Based on the proposed formula and method, the field-of-view errors on the retardance of a birefringent waveplate can be studied. Simulations and experiments on a MgF_2 biplate over an incident angle of 0°–8° and an azimuth angle of 0°–360° are presented and analyzed as an example. The main source of the systematic errors in the experiment is discussed, and the dominate errors

stem from the azimuth angle of the optical axis and the effective thickness of the biplate. After correction, the maximum difference between the experiments and simulations over the entire field of view is about 0.15°, which is reduced by more than one order of magnitude compared with that before correction. A strong agreement between the experiments and simulations demonstrates the validity and great potential of the presented method and the MME-based set-up for the characterization of the birefringent waveplate under an arbitrary field-of-view angle.

Acknowledgments

This work was funded by the National Natural Science Foundation of China (Grant Nos. 51727809, 51475191, 51575214, and 51525502), and the China Postdoctoral Science Foundation (Grant Nos. 2016M602288 and 2017T100546), the National Science and Technology Major Project of China (Grant No. 2017ZX02101006-004), and the Program for Changjiang Scholars and Innovative Research Team in University of China (Grant No. IRT13017).

ORCID iDs

Xiuguo Chen https://orcid.org/0000-0002-7067-5084
Shiyuan Liu https://orcid.org/0000-0002-0756-1439

References

[1] Aspnes D E 2014 Spectroscopic ellipsometry—past, present, and future *Thin Solid Films* **571** 334
[2] Gu H, Chen X, Jiang H, Zhang C and Liu S 2016 Optimal broadband Mueller matrix ellipsometer using multi-waveplates with flexibly oriented axes *J. Opt.* **18** 025702
[3] Williams P A 1999 Rotating-wave-plate Stokes polarimeter for differential group delay measurements of polarization-mode dispersion *Appl. Opt.* **38** 6508
[4] Liu L, Zeng A J, Zhu L L and Huang H J 2014 Lateral shearing interferometer with variable shearing for measurement of a small beam *Opt. Lett.* **39** 1992
[5] Lee S H, Kim M Y, Ser J I and Park J 2015 Asymmetric polarization-based frequency scanning interferometer *Opt. Express* **23** 7333
[6] West E A and Smith M H 1995 Polarization errors associated with birefringent waveplates *Opt. Eng.* **34** 1574
[7] Boulbry B, Bousquet B, Jeune B L, Guern Y and Lotrian J 2001 Polarization errors associated with zero-order achromatic quarter-wave plates in the whole visible spectral range *Opt. Express* **9** 225
[8] Lee J, Rovira P I, An I and Collins R W 2001 Alignment and calibration of the MgF_2 biplate compensator for applications in rotating-compensator multichannel ellipsometry *J. Opt. Soc. Am.* A **18** 1980
[9] Dong H, Tang M and Gong Y D 2012 Measurement errors induced by deformation of optical axes of achromatic waveplate retarders in RRFP Stokes polarimeters *Opt. Express* **20** 26649
[10] Dai H and Yan C X 2014 Measurement errors resulted from misalignment errors of the retarder in a rotating-retarder complete Stokes polarimeter *Opt. Express* **22** 11869
[11] Bass M and Mahajan V N 2010 *Handbook of Optics: Geometrical and Physical Optics, Polarized Light, Components and Instruments* 3rd edn vol 1 (New York: McGraw-Hill)
[12] Hale P D and Day G W 1988 Stability of birefringent linear retarders (waveplates) *Appl. Opt.* **27** 5146
[13] Nomura H and Furutono Y 2008 Polarimetry of illumination for 193 nm immersion lithography *Microelectron. Eng.* **85** 1671
[14] Simon M C 1983 Ray tracing formulas for monoaxial optical components *Appl. Opt.* **22** 354
[15] Simon M C and Gottschalk K V 1998 Optical path in birefringent media and Fermat's principle *Pure Appl. Opt.* **7** 1403
[16] Simon M C and Gottschalk K V 2007 Waves and rays in uniaxial birefringent crystals *Optik* **118** 457
[17] Chipman R A 1995 Mechanics of polarization ray tracing *Opt. Eng.* **34** 1636
[18] Liang Q T 1990 Simple ray tracing formulas for uniaxial optical crystals *Appl. Opt.* **29** 1008
[19] Zhang W Q 1992 General ray tracing formulas for crystal *Appl. Opt.* **31** 7328
[20] Zhang W Q 2000 New phase shift formulas and stability of waveplate in oblique incident beam *Opt. Commun.* **176** 9
[21] Zhu X N 1994 Explicit Jones transformation matrix for a tilted birefringent plate with its optic axis parallel to the plate surface *Appl. Opt.* **33** 3502
[22] Yang T, Wan X K, Jing H M and Liu D H 2007 An improved Jones matrix for a birefringent plate with optical axis parallel to the surface *J. Opt. A: Pure Appl. Opt.* **9** 222
[23] Avendano-Alejo M, Stavroudis O N and Goitia A R B Y 2002 Huygens's principle and rays in uniaxial anisotropic media. I. Crystal axis normal to refracting surface *J. Opt. Soc. Am.* A **19** 1668
[24] Avendano-Alejo M and Stavroudis O N 2002 Huygens's principle and rays in uniaxial anisotropic media. II. Crystal axis orientation arbitrary *J. Opt. Soc. Am.* A **19** 1674
[25] Avendano-Alejo M 2005 Analysis of the refraction of the extraordinary ray in a plane-parallel uniaxial plate with an arbitrary orientation of the optical axis *Opt. Express* **13** 2549
[26] Avendano-Alejo M and Rosete-Aguilar M 2006 Optical path difference in a plane-parallel uniaxial plate *J. Opt. Soc. Am.* A **23** 926
[27] Veriras F E, Perez L I and Garea M T 2010 Phase shift formulas in uniaxial media an application to waveplates *Appl. Opt.* **49** 2769
[28] Aleman-Castaneda L A and Rosete-Aguilar M 2016 Deviation from orthogonal polarization for ordinary and extraordinary rays in uniaxial crystals *J. Opt. Soc. Am.* A **33** 677
[29] Vilas J L and Lazarova-Lazarova A 2017 A simple analytical method to obtain achromatic waveplate retarders *J. Opt.* **19** 045701
[30] Zhang P, Tan Y D, Liu W X and Chen W X 2013 Methods for optical phase retardation measurement: a review *Sci. China Tech. Sci.* **56** 1155
[31] Lo Y L, Lin J F and Lee S Y 2004 Polariscope for simultaneous measurement of the principal axis and the phase retardation by use of two phase-locked extractions *Appl. Opt.* **43** 6248
[32] Lo Y L, Lai C H, Lin J F and Hsu P F 2004 Simultaneous absolute measurements of principal angle and phase retardation with a new common-path heterodyne interferometer *Appl. Opt.* **43** 2013

[33] Jeng Y T and Lo Y L 2006 Heterodyne polariscope for sequential measurements of the complete optical parameters of a multiple-order wave plate *Appl. Opt.* **45** 1134
[34] Lo Y L, Chih H W, Yeh C Y and Yu T C 2006 Full-field heterodyne polariscope with an image signal processing method for principal axis and phase retardation measurements *Appl. Opt.* **45** 8006
[35] Yu T C, Shan H, Pham T T H and Lo Y L 2009 Full-field and full-range sequential measurement of the slow axis angle and phase retardation of linear birefringent materials *Appl. Opt.* **48** 4568
[36] Chou C, Huang Y C and Chang M 1997 Effect of elliptical birefringence on the measurement of the phase retardation of a quartz wave plate by an optical heterodyne polarimeter *J. Opt. Soc. Am.* A **14** 1367
[37] Hsieh C H, Tsai C C, Wei H C, Yu L P, Wu J S and Chou C 2007 Determination of retardation parameters of multiple-order wave plate using a phase-sensitive heterodyne ellipsometer *Appl. Opt.* **46** 5944
[38] Tsai C C, Wei H C, Hsieh C H, Wu J S, Lin C E and Chou C 2008 Linear birefringence parameters determination of a multi-order wave plate via phase detection at large oblique incidence angles *Opt. Commun.* **281** 3036
[39] Williams P A, Rose A H and Wang C M 1997 Rotating-polarizer polarimeter for accurate retardance measurement *Appl. Opt.* **36** 6466
[40] Chakraborty B 2008 A new method for spectral performance evaluation of a chromatic and achromatic quarter-wave retarder *IEEE Trans. Instrum. Meas.* **57** 1133
[41] Chakraborty B and Chakraborty S 2016 Effect of tilt on the performance of a quarter-wave prism retarder *Opt. Eng.* **55** 094102
[42] Liu S, Chen X and Zhang C 2015 Development of a broadband Mueller matrix ellipsometer as a powerful tool for nanostructure metrology *Thin Solid Films* **584** 176
[43] Phan Q H and Lo Y L 2016 Characterization of optical/physical properties of anisotropic thin films with rough surfaces by Stokes-Mueller ellipsometry *Opt. Mater. Express* **6** 1774
[44] Gu H, Liu S, Chen X and Zhang C 2015 Calibration of misalignment errors in composite waveplates using Mueller matrix ellipsometry *Appl. Opt.* **54** 684
[45] Clarke D 2004 Interference effects in compound and achromatic wave plates *J. Opt. A: Pure Appl. Opt.* **6** 1041
[46] Dodge M J 1984 Refractive properties of magnesium fluoride *Appl. Opt.* **23** 1980